LIMIT MECHANISMS FOR ICE LOADS: FEM-DEM AND SIMPLIFIED LOAD MODELS

JANNE RANTA, ARTTU POLOJÄRVI AND JUKKA TUHKURI

Aalto University
Department of Mechanical Engineering
P.O. Box 14300, FI-00076 AALTO, Finland
e-mail: arttu.polojarvi@aalto.fi

Key words: FEM-DEM, Force Chain Buckling, Local Crushing, Ice Mechanics

Abstract. This work summarizes our recent findings on mechanisms and limits for the ice loads on wide inclined Arctic marine structures, like drilling platforms or harbour structures. The fresults presented are based on hundreds of two-dimensional combined finite-discrete element method (FEM-DEM) simulations on ice-structure interaction process. In such processes, a floating sea ice cover, driven by winds and currents, fails against a structure and fragments into a myriad of ice blocks which interact with each other and the structure. The ice load is the end result of this interaction process. Using the simulation data, we have studied the loading process, analysed the statistic of ice loads, and recently introduced a buckling model [1] and extended it to a simple probabilistic limit load model and algorithm [2], which predict the peak ice load values with good accuracy. These models capture and quantify the effect of two factors that limit the values of peak ice loads in FEM-DEM simulations: The buckling of force chains and local ice crushing in ice-to-ice contacts. The work here describes the models and demonstrates their applicability in the analysis of ice-structure interaction.

1 INTRODUCTION

Development of safe Arctic operations, such as marine transportation, offshore wind energy and offshore drilling, requires reliable prediction of maximum sea ice loads. The ice loads arise from a complex and stochastic ice-structure interaction process. This paper uses 2D combined finite-discrete element method (2D FEM-DEM) simulations to study the mechanisms that limit peak ice loads on wide, inclined, structures. Particle based methods, such as DEM and FEM-DEM, allow detailed studies on complex ice loading scenarios and they are often used in ice engineering [3]. Figure 1 illustrates our simulations, which have a floating and continuous ice sheet pushed against an inclined rigid structure. The initially intact ice sheet fails into a rubble pile of ice blocks, which interact with each other and the structure.

An important feature of discrete element simulations is that they can describe force chains [4]. In the case of ice-structure interaction, the force chains are chainlike groups of
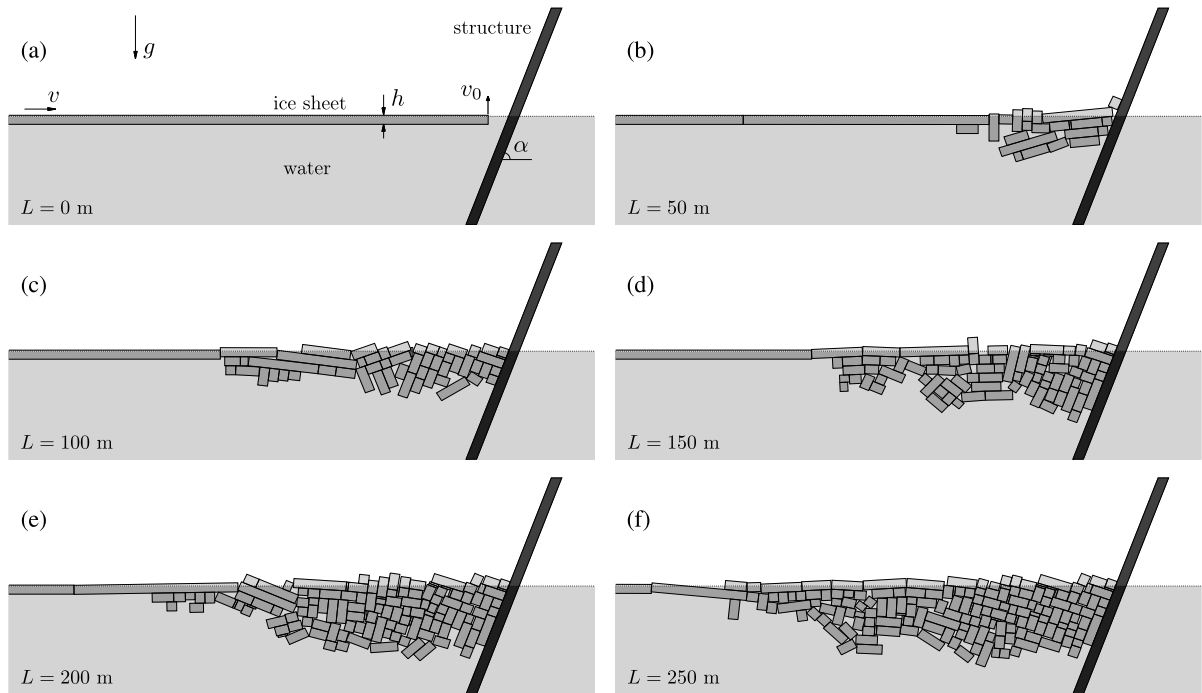
Figure 1: Snapshots of a 2D FEM-DEM-simulated ice-structure interaction process described by the length L of the ice pushed against an inclined structure. The ice sheet moves with velocity v and breaks into ice blocks in the vicinity of the structure. Broken ice forms an ice rubble pile in front of the structure. The first figure shows the initial vertical velocity perturbation v_0. Ice sheet thickness h was 1.25 m here. Figure is from [9]

ice blocks, or ice floes, that transmit the loads from the intact ice sheet to the structure. Figure 2 shows a maximum peak ice load event, in which the ice load is transmitted to the structure through a force chain. Paavilainen and Tuhkuri [5] observed that force chains exists within the ice rubble mass during peak ice load events.

This paper describes how to quantify the effects of force chain buckling and local ice crushing on maximum ice loads using fairly simple mechanical models. We first describe our simulations and a simple buckling model that captures the effect of force chain buckling. We demonstrate that the model predicts the peak ice loads in our simulations and yields plausible ice floe size predictions. Then we briefly discuss how the model can be extended to account for the local crushing of ice in contacts. The paper summarizes the work presented in detail in Ranta et al. [1] and Ranta and Polojärvi [2].

2   SIMULATIONS

The model is based on 2D FEM-DEM simulations, performed with an in-house code of Aalto University ice mechanics group. The code is based on the models described in Hopkins [6] and Paavilainen et al. [7] and its results were validated by Paavilainen et al. [7] and Paavilainen and Tuhkuri [8]. Figures 1a-f describe our simulations, in which an ice sheet of thickness h pushed against an inclined rigid structure with a constant horizontal
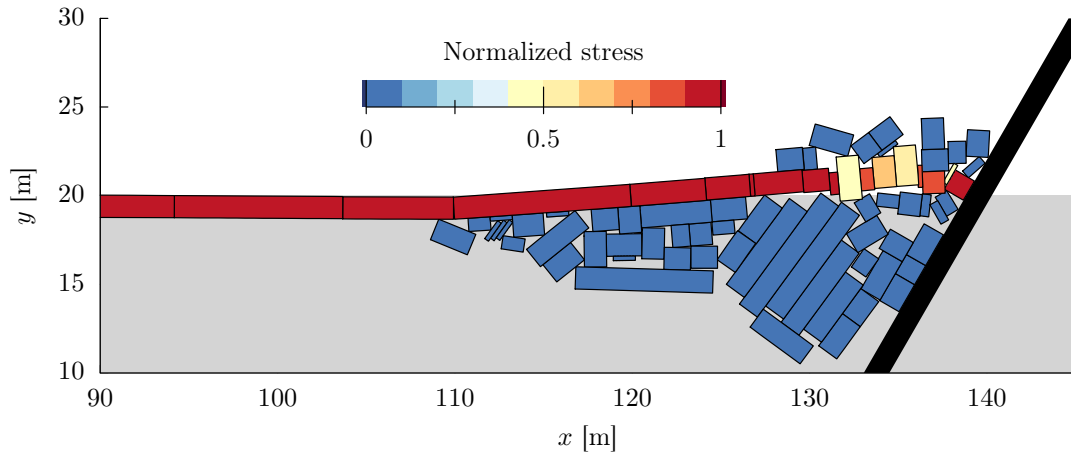
Figure 2: Snapshot from a simulation showing a force chain — a sequence of ice blocks in contact due to high compressive stress — transmitting the load from the intact ice sheet, moving towards the structure from the left. Colors indicate the normalized particle stress [4]. Figure is from [2].

velocity $v = 0.05$ m/s. Approximately 100 m from the structure, a viscous damping boundary condition is used to mimic a semi-infinite ice sheet. The sheet itself consists of rectangular discrete elements connected by viscous-elastic Timoshenko beams, which fail at locations where the beams meet a pre-defined failure criterion [10]. The beams went through a cohesive softening process upon failure [11], with the energy dissipated due to this process matching that of the fracture energy of ice [12]. Table 1 gives the main parameters of the simulations.

Contact forces were solved using an elastic-viscous-plastic normal contact force model, together with an incremental tangential contact force model with Coulomb friction [6, 7]. The model describes local crushing at ice-block-to-ice-block and ice-structure contacts. The amount of local crushing was governed by the plastic limit parameter, σ_p, which relates the maximum contact load to the contact geometry. Plastic limit parameter σ_p accounts for the local crushing between the contacting ice blocks. No new ice features were created, nor did the block geometries change during the local crushing. Water was accounted for by applying a buoyant force and simplified drag model.

The load model development was based on 350 simulations with Table 1 giving the parameters of the simulations and Table 2 summarizing the seven simulations sets, S1...S7. Each set contained 50 simulations where all parameters were constant, but the initial conditions slightly differed: An initial vertical velocity of the order of 10^{-12} m/s was applied at the free edge of the ice sheet at the start of the simulation (see [13] for details). Simulations within each set, differing by their initial conditions only, produced different ice loading processes (Figure 3) and different maximum peak ice load F^p values. As shown in Table 2, the simulation sets S1...S6 differed from each other by the values of h and σ_p. Simulation set S7 had thick ice, $h = 1.25$ m, and a high value of 8 MPa for σ_p.
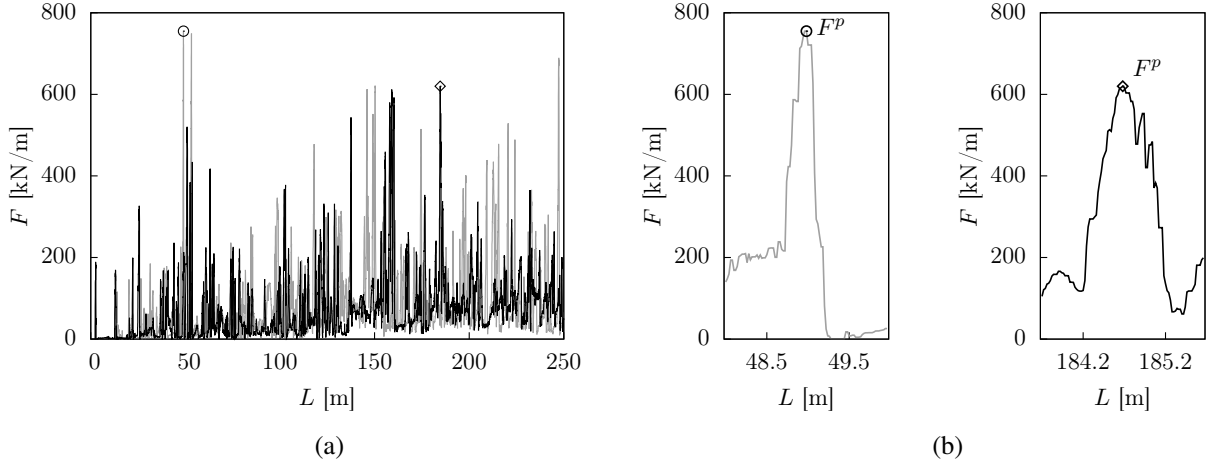
Figure 3: Two ice load F-records from two simulations with same parameterization but different initial conditions: (a) F plotted against length of pushed ice, L, and (b) close-ups of the maximum peak ice load, F^p, events. The value of F^p differs between the simulations. Here the ice thickness $h = 1.25$ m and the plastic limit $\sigma_p = 1$ MPa. Figure is from [2].

BUCKLING MODEL

In Ranta et al. [1] we showed that a simple buckling model can be used to describe how force chain buckling limits the ice load values on a wide, inclined, structure. The model, shown in Figure 4, consists of a rigid system of ice floes, having a total length of L_f, lying on an equilibrium on an elastic foundation. The modulus k of the elastic foundation,

Table 1: Main simulation parameters. The parameter values were mostly chosen following [14].

|	Description and symbol		Unit	S1…S7
General	Gravitational acceleration	g	m/s^2	9.81
	Ice sheet velocity	v	m/s	0.05
	Drag coefficient	c_d		2.0
Ice	Thickness	h	m	0.5, 0.875, 1.25
	Effective modulus	E	GPa	4
	Poisson's ratio	ν		0.3
	Density	ρ_i	kg/m^3	900
	Tensile strength	σ_f	MPa	0.6
	Shear strength	τ_f	MPa	0.6
Contact	Plastic limit	σ_p	MPa	1.0, 2.0, 8.0
	Ice-ice friction coefficient	μ_{ii}		0.1
	Ice-structure friction coefficient	μ_{iw}		0.1
Water	Density	ρ_w	kg/m^3	1010
Structure	Slope angle	α	deg	70
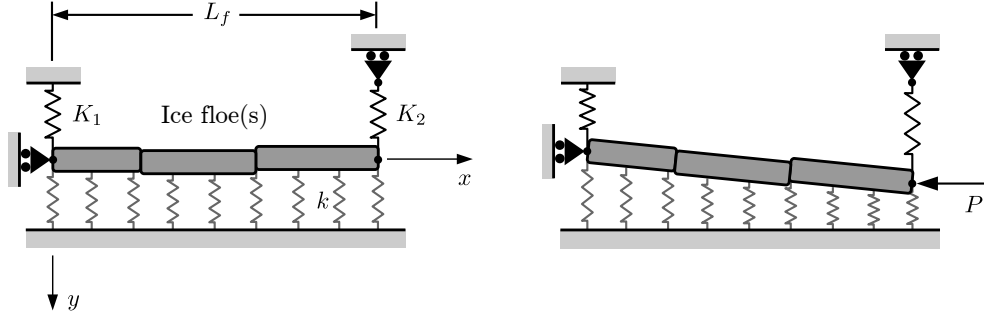
Figure 4: The buckling model we used in its initial (left) and buckled (right) states. The model consisted of a rigid ice floe of length L_f resting on an elastic foundation with modulus k presenting water. Springs K_1 and K_2 modeled the boundary conditions for the buckling modes of Table 3. Compressive force P is due to the other floes or the structure. Figure is from [2].

chosen after the specific weight of water, was $\rho_w g$, where ρ_w is the mass density of the water and g the gravitational acceleration.

The buckling model can describe different buckling modes depending on the values of the spring constants K_1 and K_2 of the springs at the ends of the floe. Table 3 shows the different modes together with the corresponding K_1 and K_2 values. Out of the four modes of the table, modes 1 and 2 assume that the elastic bending of the intact ice sheet does not have a role in a peak load event. Modes 3 and 4, on the other hand, assume that the elastic ice sheet behind the buckling floe generates a lateral support for the left end of it. The buckling load P for the model is [1]

$$P = \frac{k^2 L_f^3 + 4k(K_1 + K_2)L_f^2 + 12K_1K_2L_f}{12(kL_f + K_1 + K_2)}.$$ (1)

The characteristic length $L_c = \sqrt[4]{4EI/k}$ of a beam on elastic foundation [15] is introduced into Equation 1 by substitution of $L_f = \chi L_c$, where χ is a dimensionless buckling

Table 2: Simulation sets S1...S7 of this study. The able also shows the number N and the indices (ID) of the simulations in each set. More detailed list of simulation parameters is given in Table 1.

Set	IDs	N	h [m]	σ_p [MPa]
S1	1-50	50	0.5	1
S2	51-100	50	0.5	2
S3	101-150	50	0.875	1
S4	151-200	50	0.875	2
S5	201-250	50	1.25	1
S6	251-300	50	1.25	2
S7	301-350	50	1.25	8

length factor. L_c and χ allow expressing P for all buckling modes of Table 3 in form

$$P = a(\chi)\sqrt{kEI}, \qquad (2)$$

where a is a buckling-mode-dependent dimensionless multiplier given in Table 3. This equation can be used to study the relation between buckling and peak loads as follows. The F^p values from all simulations (Figure 3), together with the simulation parameters (k, E and I), are collected and substituted to the previous equation, which is then solved for $a(\chi) = F^p/\sqrt{kEI}$. If the simple buckling model describes well how force chain buckling limits the values of F^p, the a values for all simulations should be approximately equal; the F^p values should become normalized by factor $\sqrt{kEI}$.

3   RESULTS AND DISCUSSION

Figure 5a shows the maximum peak ice load F^p values (Figure 3a and b) from our FEM-DEM simulations. Additionally, it shows the mean F^p values with their standard deviations for the simulations of each set, S1...S7 (Table 2). While the F^p values from the simulations in a given set show scatter, the mean F^p values of the sets S1...S7 differed considerably, by up to about 500 %, mainly due to a difference in ice thickness h between the sets.

The simulations of set S7 with high σ_p yielded larger values than sets S5 and S6 with the same ice thickness $h = 1.25$ m. The values of a, solved by normalizing the F^p data of Figure 5a by factor $\sqrt{kEI}$, are shown in Figure 5b. These indicate that the peak load events were related to buckling: All mean values of a are in the same range and there is no dependency between a and h. Nonetheless, the data shows scatter not explained by the buckling model as, for example, the mean a value is clearly larger for set S7 having high σ_p.

As a appears somewhat constant, we can solve χ to estimate the lengths $L_f = \chi L_c$

Table 3: Four buckling modes considered in our study with the corresponding spring constants K_1 and K_2 (Figure 4). The buckling load $P = a(\chi)\sqrt{kEI}$, where a is a mode-dependent multiplier. Factor χ gives the buckling length as described in the text. Table is from [1]

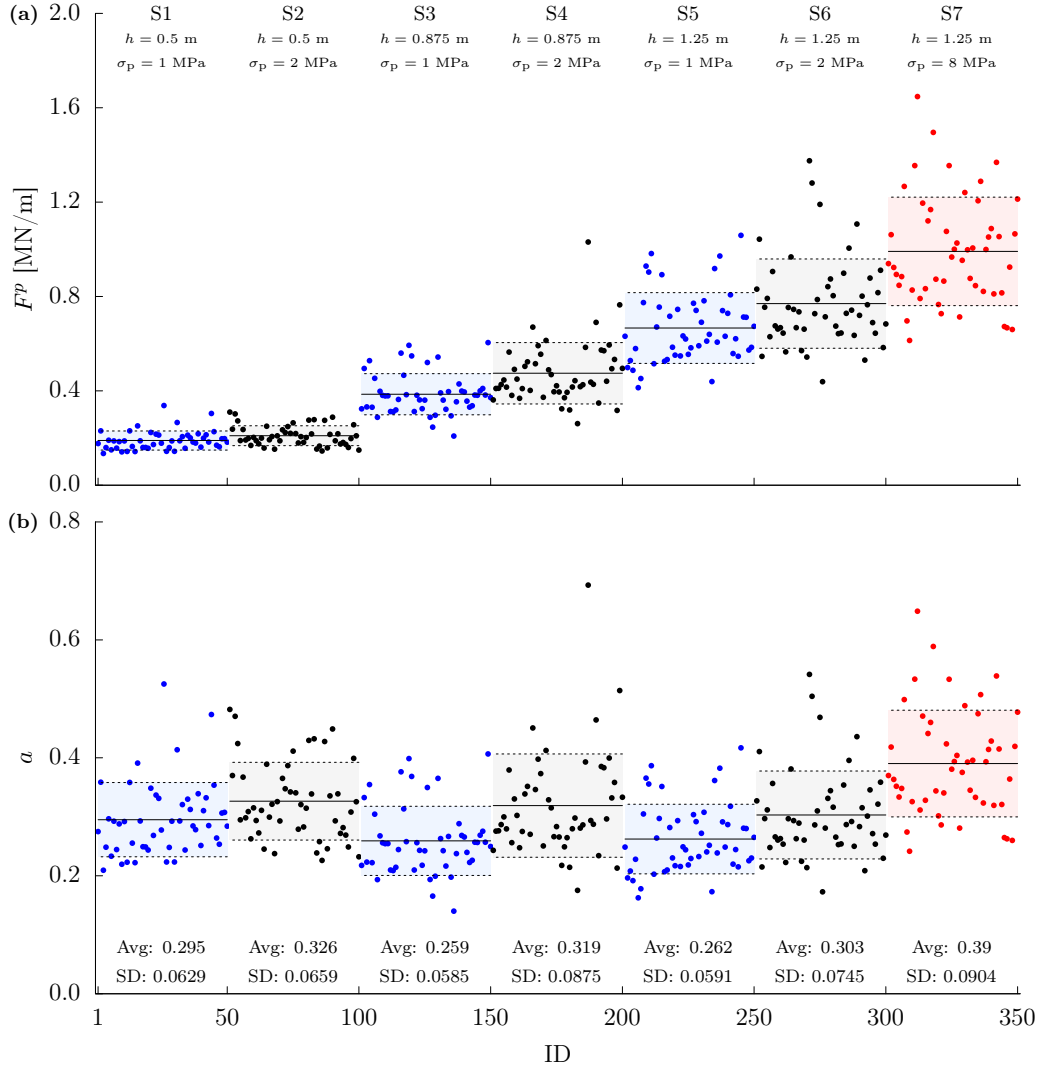| mode		K_1	K_2	a
1		0	0	$\dfrac{\chi^2}{6}$
2		∞	0	$\dfrac{2\chi^2}{3}$
3		$\dfrac{1}{2}kL_c - \dfrac{3}{4}\dfrac{P}{L_c}$	∞	$\dfrac{12\chi + 8\chi^2}{9\chi + 12}$
4		$kL_c - \dfrac{P}{2L_c}$	∞	$\dfrac{12\chi + 4\chi^2}{3\chi + 6}$

Figure 5: The values of (a) maximum peak ice load F^p values from all simulations (sets S1 ... S7, Table 2) and (b) dimensionless a factors derived using F^p data. In addition to the data points, the graphs show the mean values (Avg, solid lines) and standard deviations (SD, dashed lines) for the data.

of buckling floes. Figure 6 illustrates how the ice floes, having been compressed between the ice sheet and the structure, have gone through a buckling-like failure between the two time instances. The data points of Figure 7 are the χ values from all simulations in sets S1...S6 for modes 2-4 of Table 3. (For each a value, we get four values for χ, one for each mode, as described by Table 3.) The mean χ value for mode 1 was 1.32 ± 0.2, but χ factors for mode 1 are not shown in the figure, as this mode is physically unfeasible. It is justified to assume $L_f < L_c$, as the floes breaking off of the intact ice sheet in bending (occurring prior the peak load event) would have the length of about L_c at maximum.

The two horizontal lines of Figure 7a correspond to the χ values, which we calculated for the reported minimum and maximum values for average breaking lengths of an ice
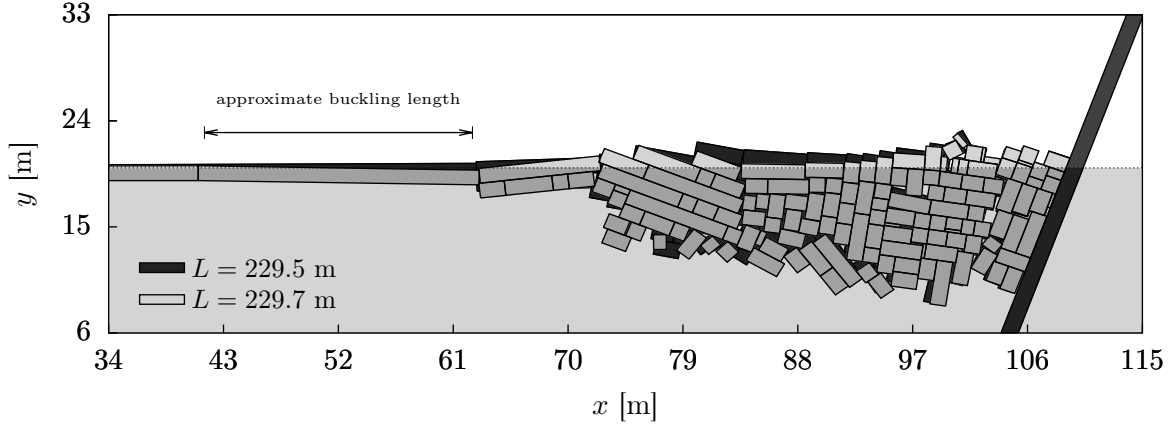
Figure 6: An example of a peak ice load event, which this simulation reached at $L = 229.5$ m. The figure also shows the model at $L = 229.7$ m (four seconds later). Buckling occurred at $x \approx 61$ m. The line in the figure illustrates the approximate buckling length. Here h and the plastic limit σ_p were 1.25 m and 2 MPa, respectively. Figure is from [1].
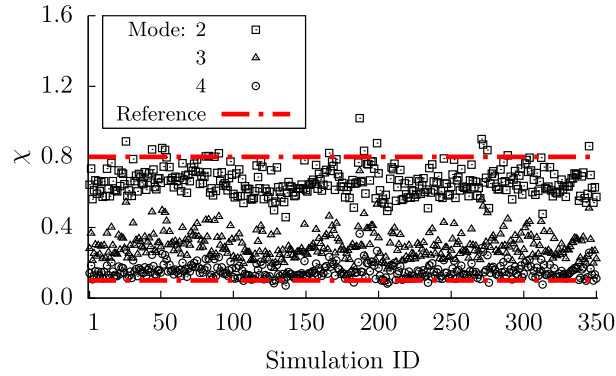

Figure 7: The dimensionless χ factor values for buckling modes 2 and 4 of Table 3 using the a values of Figure 5b. The two horizontal dash-dot lines correspond to full-scale observations on maximum and minimum breaking lengths [18]. Figure is from [1].

sheet in a full-scale ice-structure interaction process [16, 17, 18] . The figure shows that almost all of the χ values resulting from the simulated ice-structure interaction processes fall between these limits. This gives confidence on both, our simulation results and on our simplified buckling load model.

The above-described buckling model does not account for the effect of compressive strength of ice, σ_p, on the results, which would allow the buckling model to yield peak load values exceeding the compressive capacity of the ice. The lack of the effect of σ_p leads to the mean of a showing a systematic change with a change in σ_p (Figure 5b): Increase in σ_p leads to increase in a when h is kept constant. The so-called probabilistic limit load model, described in detail in Ranta and Polojärvi [2], extends the buckling model by (1) supplementing the buckling model with a local crushing model and (2) by accounting for the stochasticity in the contact geometries of the blocks belonging to the force chains.

An elementary unit of the model is one contact interface between a pair of ice blocks
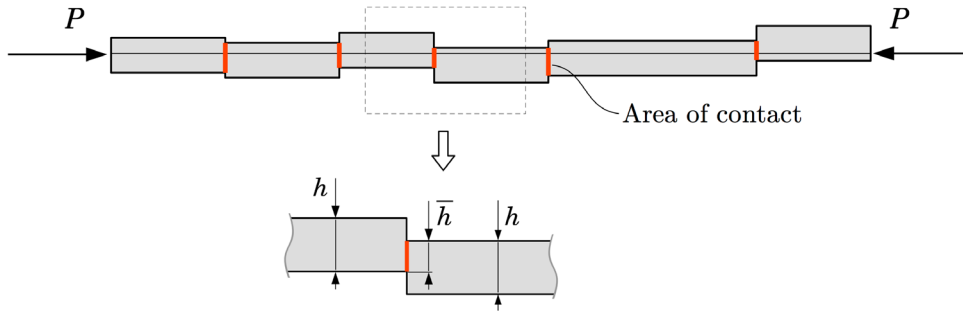
Figure 8: Force chain transmitting a load P and one contact interface between a pair of ice blocks, an elementary unit of the probabilistic limit load model. Blocks are of thickness h and the contact has a length of $\bar{h}$. Figure is from [2].

belonging to a force chain (Figure 8). The blocks are in a partial face-to-face contact due to a compressive load P. Local crushing is assumed to occur in a contact interface when $P \geq \bar{h}\sigma_p$, where $\bar{h}$ is the length of the contact interface and σ_p is the limit for compressive stress. In Ranta and Polojärvi [2] we show that this model for crushing, even with a simple triangular distribution for the contact lengths $\bar{h}$, leads to the model being able to capture the combined effect of h and σ_p on peak ice loads.

4 CONCLUSIONS

This paper summarized our work on limiting mechanisms on ice loads on inclined structure [1, 2]. The peak ice load data from ice-inclined structure processes was normalized with good accuracy by multiplying the load values with $1/\sqrt{h^3}$. This suggests that the peak ice loads in ice-inclined structure interaction process are governed by buckling. The buckling model quantifies the force chain buckling-related peak ice load values in an ice-inclined structure interaction process with fair accuracy.

The extension of the model to cover the effect of local ice crushing was also shortly discussed. The extended model accounts for a mixed-mode ice failure process where the root cause of ice failure can be due to either ice buckling or local crushing. Here we only briefly described the use of the extended model, but more details can be found from [2], where the model is even further extended into an algorithm, capable of producing large amounts of virtual ice load data that compares fairly well with full-scale observations. We believe the simple load limit load models have potential of yielding insight for the analysis of complex ice-structure interaction processes.

REFERENCES

[1] Ranta, J., Polojärvi, A., Tuhkuri, J. Limit mechanisms for ice loads on inclined structures: Buckling. *Cold Regions Science and Technology* (2018) 147:34-44.

[2] Ranta, J., Polojärvi, A. Limit mechanisms for ice loads on inclined structures: Local crushing. *Marine Structures* (2019) 67, 102633.

[3] Tuhkuri, J., Polojärvi, A. A review of discrete element simulation of ice-structure interaction. *Philosophical Transactions of the Royal Society A: Mathematical, Physical and Engineering Sciences* (2018) 376 (2129), art. no. 20170335.

[4] Peters, J., Muthuswamy, M., Wibowo, J., Tordesillas, A. Characterization of force chains in granular material. *Physical Review E - Statistical, Nonlinear, and Soft Matter Physics* (2005) 72(4)

[5] Paavilainen, J., Tuhkuri, J. Pressure distributions and force chains during simulated ice rubbling against sloped structures. *Cold Regions Science and Technology* (2013) 85:157-174.

[6] Hopkins, M. Numerical simulation of systems of multitudinous polygonal blocks. *Tech. Rep. 92–22; Cold Regions Research and Engineering Laboratory, CRREL* (1992)

[7] Paavilainen, J., Tuhkuri, J., Polojärvi, A. 2D combined finite-discrete element method to model multi-fracture of beam structures. *Engineering Computations* (2009) 26(6):578-598.

[8] Paavilainen, J., Tuhkuri, J. Parameter effects on simulated ice rubbling forces on a wide sloping structure. *Cold Regions Science and Technology* (2012) 81:1-10.

[9] Ranta, J., Polojärvi, A., Tuhkuri, J. The statistical analysis of peak ice loads in a simulated ice-structure interaction process. *Cold Regions Science and Technology* (2017) 133;46–55.

[10] Schreyer, H., Sulsky, D., Munday, L., Coon, M., Kwok, R. Elastic–decohesive constitutive model for sea ice. *Journal of Geophysical Research: Oceans* (2006) 111(11).

[11] Hillerborg, A., Modéer, M., Petersson, P.E. Analysis of crack formation and crack growth in concrete by means of fracture mechanics and finite elements. *Cement and Concrete Research* (1976) 6:773–782.

[12] Dempsey, J., Adamson, R., Mulmule, S. Scale effects on the in-situ tensile strength and fracture of ice. Part II: first-year sea ice at resolute, N.W.T. *International Journal of Fracture* (1999);95:347–366.

[13] Ranta, J., Polojärvi, A., and Tuhkuri, J. Ice loads on inclined marine structures - virtual experiments on ice failure process evolution. *Marine Structures* (2018) 57:72-86.

[14] Timco, G., Weeks, W. A review of the engineering properties of sea ice. *Cold Regions Science and Technology* (2010) 60(2):107129.

[15] Hetényi, M. *Beams on elastic foundation: Theory with applications in the fields of civil and mechanical engineering.* Ann Arbor: The University of Michigan Press (1979).

[16] Lau, M., Molgaard, J., Williams, F., and Swamidas, A. An analysis of ice breaking pattern and ice piece size around sloping structures. *In Proceedings of OMAE99, 18th International Conference on Offshore Mechanics and Arctic Engineering* (1999) 199-207.

[17] Frederking, R. Dynamic ice force on an inclined structure. *In Physics and Mechanics of Ice. IUTAM Symposium* (1980) 104116.

[18] Li, F., Yue, Q., Shkhinek, K., and Kärnä , T. A qualitative analysis is of breaking length of sheet ice against conical structures. *In Proceedings of the 17th International Conference on Port and Ocean Engineering under Arctic Conditions (POAC03)* (2003) 293-304.